

This is a non-peer reviewed pre-print submitted to EarthArxiv.
Subsequent peer-reviewed versions of this manuscript may have slightly different content. The authors welcome feedback.

Please contact Sandy H. S. Herho (sandy.herho@email.ucr.edu) regarding this manuscript's content.

imc-precip-iso: Open monthly stable isotope data of precipitation over the Indonesian Maritime Continent

R. Suwarman¹, S. H. S. Herho^{2,3,*}, H. A. Belgaman⁴, D. E. Irawan⁵, K. Ichiyanagi⁶, I. M. Yosa¹, A. I. D. Utami⁷, S. Prayogo⁸, and E. Aldrian⁴

¹Atmospheric Science Research Group, Bandung Institute of Technology (ITB), Bandung, Indonesia

²Department of Earth and Planetary Sciences, University of California, Riverside, USA

³Department of Geology, University of Maryland, College Park, USA

⁴Research Center for Climate and Atmosphere (PRIMA), National Research and Innovation Agency (BRIN), Bandung, Indonesia

⁵Applied Geology Research Group, Bandung Institute of Technology (ITB), Bandung, Indonesia

⁶Faculty of Advanced Science and Technology, Kumamoto University, Kumamoto, Japan

⁷Indonesian Meteorology, Climatology, and Geophysical Agency (BMKG), Jakarta, Indonesia

⁸Software Engineering Division, Manvis Teknologi Engineering, Bandung, Indonesia

*Corresponding author: sandy.herho@email.ucr.edu

Abstract

Stable isotopes, $\delta^2\text{H}$, $\delta^{18}\text{O}$, and d-excess, are valuable tools as natural tracers of diffusion processes and phase changes in the global hydroclimatological cycle. The Indonesian Maritime Continent (IMC) is an archipelago area surrounded by very warm waters which induce convective activities as the primary heat source driving global atmospheric circulation. Given the central role of IMC in this hydroclimatological cycle, comprehensive study and data collection on the stable isotopes of precipitation in this region is crucial.

In this study, we collected monthly stable isotope data from 62 stations spread throughout the Indonesian archipelago from September 2010 to September 2017. We cleaned the data and conducted quality control activities by comparing the Local Meteoric Water Line (LMWL) to previous studies in a similar climatic region. We shared these data openly on our GitHub repository, making them easier to update and interact with users in the future.

1 INTRODUCTION

Indonesian Maritime Continent (IMC) comprises a group of islands surrounded by the Indian and Pacific Oceans. The region's climate is influenced by its insular geography and its position near the Equator. Located in the western part of the Indo-Pacific warm pool (IPWP), IMC is a source of latent heat release and deep convection which drives the Hadley and Walker cells, thus playing an essential role in the earth's hydrological cycle (Yang et al., 2019; Xue et al., 2020). IMC is also the only link for warmed surface waters from the Pacific Ocean to the Indian Ocean through the Indonesian Throughflow (ITF), a surface flow component of the global ocean conveyor belt (e. g. Godfrey, 1996; Li et al., 2020; Makarim et al., 2019; Nagai et al., 2021; Santoso et al., 2022).

In general, IMC experiences two seasons, namely the wet and dry seasons, each in boreal winter - spring (November-March/NDJFM) and boreal summer - fall (May - September/MJJAS) (Aldrian and Susanto, 2003; Yang et al., 2019). During the wet season, there is warm sea surface temperature (SST) and heavy precipitation over the IMC, which is brought by the Asian winter monsoon, which is northeasterly to the north of the equator and northwesterly to the south of the equator, the opposite also happens in the dry season (Chang et al., 2005a,b; Yang et al., 2019). Besides the annual cycle, IMC precipitation is influenced by internal global atmosphere-ocean interactions, such as the El Niño Southern Oscillation (ENSO) (e. g.

46 Peatman et al., 2021; Zhu et al., 2022; Chen et al., 2023a; Gao and Li, 2023; Lu et al., 2023) and the Indian
47 Ocean Dipole mode (IOD) (e. g. Yang et al., 2019; Hu et al., 2020; Peatman et al., 2021; Xiao et al., 2022).
48 On an intra-annual scale, precipitation over the IMC is also influenced by the Madden-Julian Oscillation
49 (MJO), which propagates from the Indian Ocean to the Pacific Ocean via IMC (e. g. Ahn et al., 2020; Wei
50 et al., 2020; Peatman et al., 2021; Bai and Schumacher, 2022; Abhik et al., 2023; Hudson and Maloney,
51 2023).

52 Given the importance of IMC in understanding the earth's hydroclimatological phenomena (Yamanaka,
53 2016), investigation of precipitation characteristics is inevitable. One of the characteristics of precipitation
54 that is important to investigate is the traditional water-stable isotopes of precipitation ($\delta^{18}\text{O}$ and $\delta^2\text{H}$)
55 which are considered one of the natural tracers of hydrological cycles as a consequence of equilibrium and
56 kinetic processes during phase transitions and diffusive processes (Tritschler et al., 2020; Valdivielso et al.,
57 2020; He et al., 2021; Malik et al., 2022). In general, oxygen-18 ($\delta^{18}\text{O}$) and deuterium ($\delta^2\text{H}$) at mid- and
58 high-latitudes are correlated with temperature (e. g. Bershaw, 2018; Liu et al., 2019; Routson et al., 2019;
59 Xia et al., 2019b, 2020). However, in tropical regions such as the IMC, these two isotopic compositions
60 show a negative correlation (e.g. Kurita et al., 2009; Munksgaard et al., 2019; Xia et al., 2019a; Jackisch
61 et al., 2022) due to a rainout process known as the amount effect (Dansgaard, 1964). $\delta^{18}\text{O}$ can also be
62 used as a signature of the water vapour transport process during ENSO and MJO over the IMC (Suwarman
63 et al., 2013; Belgaman et al., 2016b; Suwarman et al., 2017). Observations of $\delta^{18}\text{O}$ and $\delta^2\text{H}$ in the tropics are
64 also crucial to confirm the sensitivity of proxy precipitation observations in paleoclimatology using proxy
65 system modelling (PSM), which requires modern precipitation isotope data in the region (Evans et al., 2013).
66 Modern precipitation isotope observations are also needed to correct calculations performed by isotope-
67 enabled General Circulation Models (iGCMs) (e. g. Peng et al., 2020; Nan et al., 2021; Chen et al., 2022,
68 2023b).

69 Until recently, there is not much open and publicly accessible data on traditional precipitation isotope over
70 the IMC. There are four isotope stations operated by the International Atomic Energy Agency (IAEA) within
71 the framework of the Global Network of Isotopes in Precipitation (GNIP) program. However, these sta-
72 tions stopped operating in 2003 and only cover the Java region, except for the Jayapura station in Papua
73 (Belgaman et al., 2016a). In addition, there were isotope observations conducted by the Institute of Ob-
74 servational Research for Global Change (IORGC)/Japan Agency for Marine-Earth Science and Technology
75 (JAMSTEC) conducted at six stations across IMC between 2001 and 2007 (Kurita et al., 2009; Belgaman
76 et al., 2016a).

77 In this study, we conducted monthly $\delta^{18}\text{O}$ and $\delta^2\text{H}$ sampling at 62 observation stations along the IMC
78 from September 2010 to September 2017. Part of these data (30 stations) have been used in a study by
79 Belgaman et al. (2017) but has yet to be opened to the public. We opened the $\delta^{18}\text{O}$ and $\delta^2\text{H}$ measurements
80 to the public on our GitHub repository to support democratizing knowledge based on open-source code
81 and reproducible datasets (Perkel, 2016).

82 2 DATA ACQUISITION

83 We conducted field sampling from 62 meteorological and climatological stations owned by the Indonesian
84 Meteorology, Climatology, and Geophysical Agency (BMKG) throughout the IMC area (Figure 1). To find out
85 the details of station numbering and their location, see the table on the following URL: https://github.com/sandyherho/imc-precip-iso/blob/main/output_data/sta_list.csv. We collected these pre-
86 cipitation samples manually using buckets and then put them into 6 mL glass vials with screw caps. To
87 prevent secondary evaporation after storage, we discarded samples with a volume of less than 5 mL. We
88 collected these monthly precipitation samples from September 2010 to September 2017.

90 We measured $\delta^{18}\text{O}$ and $\delta^2\text{H}$ using the Picarro[®] L2120-i instrument using the cavity ring-down spectroscopy
91 technique, which has proven practical and accurate in measuring water isotopes (e. g. De Graaf et al., 2020;
92 Maithani and Pradhan, 2020; Sagayama et al., 2021; Hutchings and Konecky, 2023; Zhang and Xu, 2023).
93 We measured the ratio of the abundance of the heavy to light isotopes (R), in the context of this study,
94 $^2\text{H}/^1\text{H}$ and $^{18}\text{O}/^{16}\text{O}$, from samples by comparing them to the international standard, namely the Vienna
95 Standard Mean Ocean Water (VSMOW) (Hornberger, 1995) so that δ values were obtained in units per mil
96 (‰) using the following equation:

$$\delta = \left(\frac{R_{\text{sample}}}{R_{\text{standard}}} - 1 \right) \times 10^3 \quad (1)$$

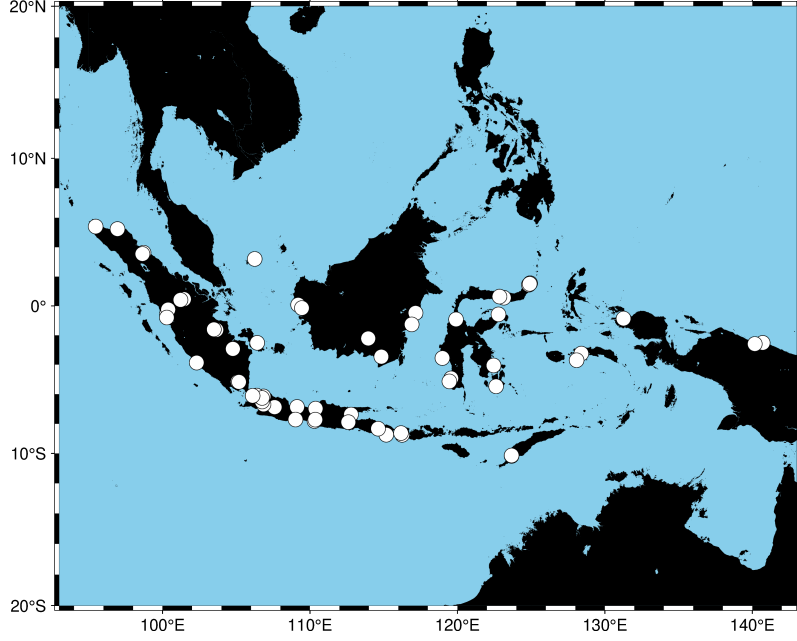


Figure 1: Location of the stations at which monthly samples of precipitation were collected for isotope measurements over the IMC (rendered using PyGMT (Wessel et al., 2019; Uieda et al., 2023)).

97 Due to the limited supply of international standards (is), we calibrated the samples (x) using three working
 98 standards (ws), Aqua Standard[®], SLW2 and ICE2, which had been calibrated against VSMOW. This calcula-
 99 tion process is formulated through the following equation (Coplen, 1988):

$$\delta_{x-is} = \delta_{x-ws} + \delta_{ws-is} + (\delta_{x-ws} \times \delta_{ws-is}) \times 10^{-3} \quad (2)$$

100 Long-term standard errors (1σ) for these $\delta^{18}\text{O}$ and $\delta^2\text{H}$ measurements are $\pm 0.08 \text{ ‰}$ and $\pm 0.22 \text{ ‰}$, re-
 101 spectively (Belgaman et al., 2017).

102 Microsoft[®] Excel files extracted from the isotope measurement instrument were then converted into a
 103 text-formatted files, i. e. comma-separated values (CSV) format to make them easier to read by various
 104 kinds of software without being limited by a paid license (Taylor, 2015; Mäs et al., 2018). These data were
 105 then splitted into time series for each station and the entire IMC. In addition, we also calculated d-excess
 106 (d), which is defined as the deviation from $\delta^2\text{H}$ to $\delta^{18}\text{O}$ according to the definition of the Global Meteoric
 107 Water Line (GMWL) (Craig, 1961), which can be written as follows:

$$d = \delta^2\text{H} - 8\delta^{18}\text{O} \quad (3)$$

108 Calculation of this d-excess is necessary, given its correlation with the oceanic source of precipitation (Merli-
 109 vat and Jouzel, 1979; Bershaw, 2018). Globally, this d-excess is a dependent variable of the relative humidity
 110 of the sea surface (Pfahl and Sodemann, 2014). Using d-excess, we can find the moisture flux anomaly dur-
 111 ing extreme events, such as ENSO influences in precipitation (e. g. Sánchez-Murillo et al., 2017; Yoshikawa
 112 et al., 2020; Shao et al., 2021). We did the entire data wrangling process using NumPy (Van Der Walt et al.,
 113 2011) and pandas (McKinney et al., 2011) libraries in the Python computing environment.

114 3 METHOD

115 We performed Local Meteoric Water Line (LMWL) calculations as part of our quality control efforts. It has
 116 been known since a study conducted by Craig (1961) that there is a linear relationship between $\delta^2\text{H}$ to $\delta^{18}\text{O}$
 117 globally, which can be formulated as follows:

$$\delta^2\text{H} = 8\delta^{18}\text{O} + 10 \quad (4)$$

118 However, local slope variations and intercepts were only discovered after collecting IAEA/GNIP observa-
 119 tions through the study of Rozanski et al. (1993), better known as LMWL. In this study, it is emphasized

120 that the relationship between the two isotopes is still linear. Variations in the slope may store information
 121 about the local seasonal climatology (Putman et al., 2019).

122 We used Bayesian Linear Regression (BLR) to determine the relationship between $\delta^2\text{H}$ and $\delta^{18}\text{O}$ over the
 123 IMC. BLR allows better handling of uncertainty in models. This method recognizes that we need perfect
 124 information about model parameters or data variability. We can represent this uncertainty using a proba-
 125 bility distribution on the parameters in the Bayesian approach. This approach helps generate more realistic
 126 and credible parameter estimates and confidence intervals. The BLR approach allows us to incorporate any
 127 prior knowledge about the model parameters. This is useful when we need more data or want to use ex-
 128 isting domain knowledge. In this study, we determined the priors for slopes and intercepts from the global
 129 data compilation for humid tropical regions (Köppen class A) that was done by Putman et al. (2019). Apart
 130 from single-point estimates (as in "frequentist" linear regression), the BLR gives a full posterior distribution
 131 of model parameters after looking at the data. This provides richer information about the parameter uncer-
 132 tainties and allows for more robust modelling of the $\delta^2\text{H}$ - $\delta^{18}\text{O}$ covariance. Because of these advantages,
 133 the Bayesian approaches have recently been popular for solving water isotope problems (e. g. Putman
 134 et al., 2019; Arellano et al., 2020; Torres-Martínez et al., 2020; Zhang et al., 2020; Kang et al., 2022; Zaryab
 135 et al., 2022; Mao et al., 2023). The full benefits of using BLR can be found in Klauenberg et al. (2015).

136 The simple linear regression model that we used to explain the statistical relationship between $\delta^2\text{H}$ and
 137 $\delta^{18}\text{O}$ is illustrated in the following equation:

$$\delta^2\text{H}_i = \beta_0 + \beta_1\delta^{18}\text{O}_i + \varepsilon_i \quad (5)$$

138 , where $\delta^2\text{H}_i$ and $\delta^{18}\text{O}_i$ are the observed deuterium and oxygen-18 isotope values for the i -th data point,
 139 respectively. β_0 and β_1 are the unknown regression coefficients (intercept and slope) to be estimated.
 140 ε_i is the random error term, assumed to be normally distributed, with mean zero and constant variance
 141 σ^2 .

142 BLR estimation started by specifying the prior distributions for the unknown parameters: β_0 , β_1 , and σ^2 . In
 143 this study, we assumed normal prior for intercept and slope, and uniform prior for variance (West, 1984):
 144

$$\begin{cases} \beta_0 \sim \mathcal{N}(m_0, s_0^2) \\ \beta_1 \sim \mathcal{N}(m_1, s_1^2) \\ \sigma^2 \sim U(a, b) \end{cases} \quad (6)$$

145 Parameters m_0 , m_1 , s_0 , s_1 , a , and b were determined from the global observation database for the humid
 146 tropical regions (Köppen class A) (Putman et al., 2019).

147 Assuming errors ε_i are normally distributed, the likelihood function can be written in the following form:

$$p(\delta^2\text{H}_i|\beta_0, \beta_1, \delta^{18}\text{O}_i, \sigma^2) = \frac{1}{\sqrt{2\pi\sigma^2}} \exp\left(-\frac{(\delta^2\text{H}_i - \beta_0 - \beta_1\delta^{18}\text{O}_i)^2}{2\sigma^2}\right) \quad (7)$$

148 The joint posterior distribution of the BLR parameters given the observed isotope data ($\delta^2\text{H}_i, \delta^{18}\text{O}_i$) is:
 149

$$p(\beta_0, \beta_1, \sigma^2|\text{data}) \propto p(\text{data}|\beta_0, \beta_1, \sigma^2) \times p(\beta_0) \times p(\beta_1) \times p(\sigma^2) \quad (8)$$

150 , where $p(\text{data}|\beta_0, \beta_1, \sigma^2)$ is the likelihood and $p(\beta_0)$, $p(\beta_1)$, and $p(\sigma^2)$ are the priors.

151 We used a simple algorithm from the Markov chain Monte Carlo (MCMC) methods (Jones and Qin, 2022),
 152 the Metropolis-Hastings (MH) algorithm (Metropolis et al., 1953; Hastings, 1970), to estimate the posterior
 153 distribution. This algorithm can approximate the posterior distribution without the need to compute the
 154 normalization constant (Chib and Greenberg, 1995). MH algorithm has also proven reliable enough to be
 155 used in hydroclimatological problems (e. g. Putman et al., 2019; Fan et al., 2022; Herho, 2022; Sharma and
 156 Mujumdar, 2022; Vinnarasi and Dhanya, 2022; Xu et al., 2022; Zolghadr-Asli et al., 2022). MH algorithm
 157 can be summarized into several steps as follows:

158 1. Initialize the parameters $\beta_0^{(0)}$, $\beta_1^{(0)}$, and $\sigma_0^{2(0)}$ to some initial values.

159 2. For iteration $t = 1$ to T , where T is the number of iterations (in this study, we used 10,000 steps
 160 with the tuning of 2,000 steps which are the "burn in" iterations used to accelerate convergence
 161 (Jones and Qin, 2022; South et al., 2022)):

162 (a) Calculate the acceptance ratio α :

$$\alpha = \frac{p(\text{data}|\beta_0, \beta_1, \sigma^{2*}) \times p(\beta_0) \times p(\beta_1) \times p(\sigma^{2*})}{p(\text{data}|\beta_0^{(t-1)}, \beta_1^{(t-1)}, \sigma^{2(t-1)}) \times p(\beta_0^{(t-1)}) \times p(\beta_1^{(t-1)}) \times p(\sigma^{2(t-1)})} \quad (9)$$

163 (b) Generate a uniform random number u from $[0, 1]$.

164 (c) If $u < \alpha$, accept the proposed parameters: $\beta_0^{(t)} = \beta_0, \beta_1^{(t)} = \beta_1, \sigma^{2(t)} = \sigma^{2*}$. Otherwise,
 165 keep the previous parameters: $\beta_0^{(t)} = \beta_0^{(t-1)}, \beta_1^{(t)} = \beta_1^{(t-1)}, \sigma^{2(t)} = \sigma^{2(t-1)}$.

166 3. After T iterations, we have samples from the posterior distribution. We use these samples to esti-
 167 mate the posterior mean, credible intervals, and other properties of the parameters.

168 This study uses a symmetrical Gaussian proposal distribution to simplify computing the acceptance ratio
 169 (Jones and Qin, 2022; Karras et al., 2022; South et al., 2022; Agrawal et al., 2023). We implemented the
 170 entire BLR process using the PyMC3 library within the Python computing environment (Salvatier et al.,
 171 2016).

172 4 RESULTS and DISCUSSION

173 The number of data points at each isotope observation station can be seen in Figure 2. The three stations
 174 with the most data collection were the Kemayoran Air Pollution Post in Jakarta (#1), with a total of 47 data
 175 points, followed by Deli Serdang in North Sumatra (#5) with a total of 46 data points, and in third place is the
 176 Bengkulu station (#11) which is located on the southwest coast of Sumatra with a total of 43 observations of
 177 data points. The stations with the fewest number of observations include Tambang (#57), located in Riau,
 178 and Ranomeeto (#58) in Southeast Sulawesi, each with two data points. Stations with the second-fewest
 179 number of observations include El Tari (#24) and Kupang in East Nusa Tenggara (#38), Mlati (#49) in Sleman,
 180 Yogyakarta, Malikusaleh (#53) in North Aceh, Koba (#56) in Bangka Belitung, each of which recorded only
 181 three data points. The stations with the third-fewest number of observations are Tarempa (#36) in the Riau
 182 Archipelago, West Seram (#48) in Maluku, and Sorong (#54) in Southwest Papua, each of which only has
 183 four data points. All stations' average and median data points were 21.968 and 22, respectively. These are
 184 very small because only about a quarter of the 85 months of observation period had successfully extracted
 185 $\delta^{2}\text{H}$ and $\delta^{18}\text{O}$ values.

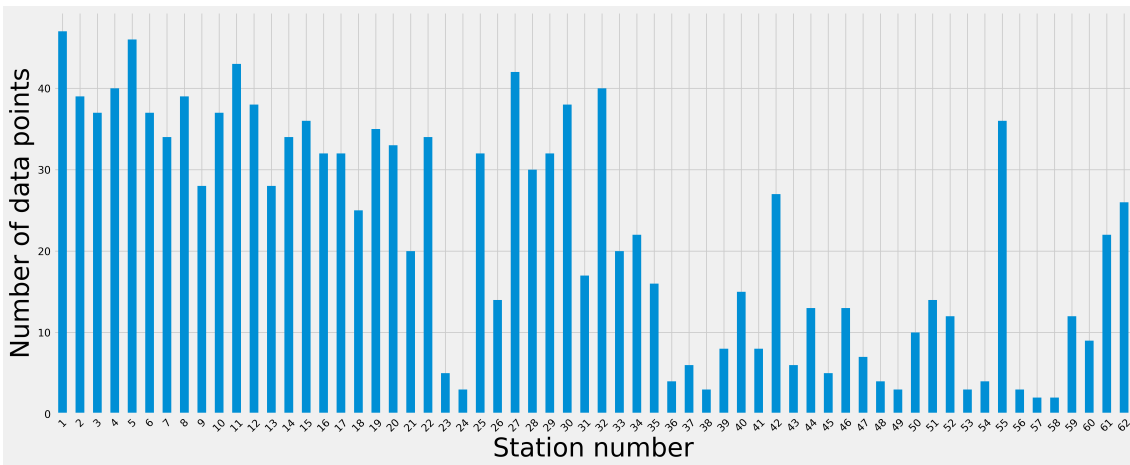


Figure 2: Availability of data points at each isotope station over the IMC collected in this study.

186 Weaknesses in data collection are also found in the need for more coverage of areas outside parts of Suma-
 187 tra and Java due to limited access to transportation for sending samples. This must be underlined because
 188 most of the isotope measurements we produced in this study are concentrated in a region with monsoonal

189 rainfall classifications (Aldrian and Susanto, 2003; Supari et al., 2018; Ferijal et al., 2021). In contrast, anti-
190 monsoonal and semi-annual regions are underrepresented. This is also evident in the less distribution of
191 $\delta^2\text{H}$ and $\delta^{18}\text{O}$ values at stations in these two regions, as shown in the boxplots in Figure 3.

192 By combining $\delta^2\text{H}$ and $\delta^{18}\text{O}$ from all stations, we performed BLR inference, where the results of trace
193 plots and the posterior distribution of the linear regression parameters can be seen in Figure 4. There is a
194 convergence of all linear regression parameters, which can be visually seen in the trace plots (Figure 4a).
195 The posterior distribution of the LMWL parameters that have been calculated using the MH algorithm is
196 shown in Figure 4b. The mean and standard deviation of the posterior intercept are 3.506 ‰ and 1.732 ‰,
197 respectively. Meanwhile, the mean and standard deviation of the posterior slope are 7.298 ‰ and 0.267
198 ‰, respectively. Then, for a 2σ credible interval, we can write the LMWL equation as follows:

$$\delta^2\text{H} = 7.298(\pm 0.534)\delta^{18}\text{O} + 3.506(\pm 3.464) \quad (10)$$

199 The two regression coefficients in Equation 10 are shallower when compared to GMWL. This indicates
200 the occurrence of a sub-cloud evaporation process which indicates the occurrence of re-evaporation from
201 rainwater after falling under the clouds through a tropical convective processes. Visually this can be seen
202 by shifting the LMWL regression line clockwise when compared to the GMWL (Figure 5). Similar things
203 were also found in previous studies over the Maritime Continent (He et al., 2018a,b, 2021).

204 5 CONCLUDING REMARKS

205 Based on water isotope observations from 62 stations that we collected from September 2010 to Septem-
206 ber 2017, we managed to build monthly $\delta^2\text{H}$, $\delta^{18}\text{O}$, and d-excess datasets per station and for all IMC, which
207 are shared openly, accessible, and easily updated on the GitHub repository. We have also performed quality
208 control on these data by calculating the LMWL using BLR, which is under the range of slopes and intercepts
209 in previous studies conducted in areas with similar climate types (e. g. He et al., 2018a,b; Putman et al.,
210 2019; He et al., 2021). The open data we shared are by far the most complete data over the IMC for stable
211 isotopes of precipitation.

212 There are limitations to this study. One of them is that we should have checked the amount effect. This
213 is due to the limitation of station precipitation data, which contains many empty data. In the future, a
214 combination of station data and other high-resolution data sources is needed, such as the Climate Hazards
215 Group InfraRed Precipitation with Station data (CHIRPS) (Funk et al., 2015), which can be used to calculate
216 the amount effect. In addition, this monthly water isotope observation activities over the IMC were stopped
217 in September 2017. This activity should be continued, given the central position of the IMC in the Earth's
218 climate system, which is currently undergoing significant changes as a consequence of the unprecedented
219 increase in anthropogenic radiative forcing. The study of water isotopes in precipitation over the IMC can
220 undoubtedly deepen our understanding of anthropogenic and natural attributions in the hydrologic cycle
221 in the tropics.

222 FUNDING

223 This study was supported by ITB Research, Community Service and Innovation Program (PPMI-ITB) and
224 Japan Society for the Promotion of Science (JSPS) KAKENHI (#24510256 and #16H05619).

225 DATA AVAILABILITY STATEMENT

226 All relevant code and data are available from this GitHub repository: [https://github.com/sandyherho/
227 imc-precip-iso](https://github.com/sandyherho/imc-precip-iso).

228 CONFLICT OF INTEREST

229 The authors declare there is no conflict.

References

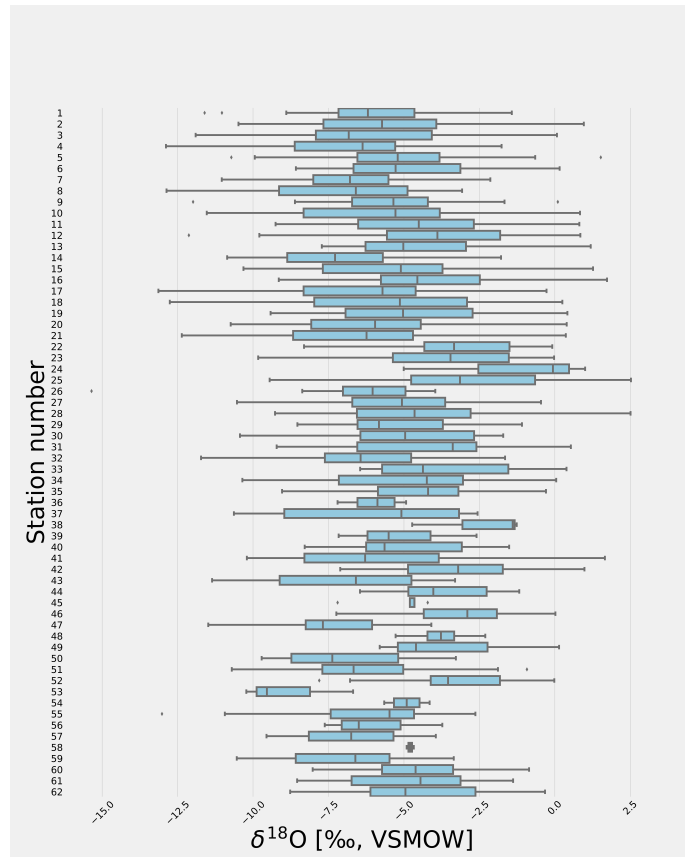
- 230
- 231 Abhik, S., Hendon, H. H., and Zhang, C. (2023). The Indo-Pacific Maritime Continent Barrier Effect on MJO
232 Prediction. *Journal of Climate*, 36(3):945–957.
- 233 Agrawal, S., Vats, D., Łatuszyński, K., and Roberts, G. O. (2023). Optimal scaling of MCMC beyond Metropo-
234 lis. *Advances in Applied Probability*, 55(2):492–509.
- 235 Ahn, M.-S., Kim, D., Ham, Y.-G., and Park, S. (2020). Role of Maritime Continent land convection on the
236 mean state and MJO propagation. *Journal of Climate*, 33(5):1659–1675.
- 237 Aldrian, E. and Susanto, R. D. (2003). Identification of three dominant rainfall regions within Indonesia and
238 their relationship to sea surface temperature. *International Journal of Climatology*, 23(12):1435–1452.
- 239 Arellano, L. N., Good, S. P., Sánchez-Murillo, R., Jarvis, W. T., Noone, D. C., and Finkenbiner, C. E. (2020).
240 Bayesian estimates of the mean recharge elevations of water sources in the Central America region using
241 stable water isotopes. *Journal of Hydrology: Regional Studies*, 32:100739.
- 242 Bai, H. and Schumacher, C. (2022). Topographic influences on diurnally driven MJO rainfall over the Mar-
243 itime Continent. *Journal of Geophysical Research: Atmospheres*, 127(6):e2021JD035905.
- 244 Belgaman, H. A., Ichianagi, K., Suwarman, R., Tanoue, M., Aldrian, E., Utami, A. I. D., and Kusumaningtyas,
245 S. D. A. (2017). Characteristics of seasonal precipitation isotope variability in Indonesia. *Hydrological
246 Research Letters*, 11(2):92–98.
- 247 Belgaman, H. A., Ichianagi, K., Tanoue, M., and Suwarman, R. (2016a). Observational research on stable
248 isotopes in precipitation over Indonesian maritime continent. *Nihon Suimon Kagaku Kaishi (Online)*,
249 46(1):7–28.
- 250 Belgaman, H. A., Ichianagi, K., Tanoue, M., Suwarman, R., Yoshimura, K., Mori, S., Kurita, N., Yamanaka,
251 M. D., and Syamsudin, F. (2016b). Intraseasonal variability of $\delta^{18}\text{O}$ of precipitation over the Indonesian
252 maritime continent related to the Madden–Julian oscillation. *SOLA*, 12:192–197.
- 253 Bershaw, J. (2018). Controls on deuterium excess across Asia. *Geosciences*, 8(7):257.
- 254 Chang, C.-P., Harr, P. A., and Chen, H.-J. (2005a). Synoptic disturbances over the equatorial South China Sea
255 and western Maritime Continent during boreal winter. *Monthly Weather Review*, 133(3):489–503.
- 256 Chang, C.-P., Wang, Z., McBride, J., and Liu, C.-H. (2005b). Annual cycle of Southeast Asia—Maritime
257 Continent rainfall and the asymmetric monsoon transition. *Journal of Climate*, 18(2):287–301.
- 258 Chen, C., Sahany, S., Moise, A. F., Chua, X. R., Hassim, M. E., Lim, G., and Prasanna, V. (2023a). ENSO–Rainfall
259 Teleconnection over the Maritime Continent Enhances and Shifts Eastward under Warming. *Journal of
260 Climate*, 36(14):4635–4663.
- 261 Chen, J., Chen, J., Zhang, X. J., Peng, P., and Risi, C. (2022). A 148-year precipitation oxygen isoscape for
262 China generated based on data fusion and bias correction of iGCMs simulations. *Earth System Science
263 Data Discussions*, pages 1–27.
- 264 Chen, J., Chen, J., Zhang, X. J., Peng, P., and Risi, C. (2023b). A century and a half precipitation oxygen
265 isoscape for China generated using data fusion and bias correction. *Scientific Data*, 10(1):185.
- 266 Chib, S. and Greenberg, E. (1995). Understanding the Metropolis-Hastings Algorithm. *The American statisti-
267 cian*, 49(4):327–335.
- 268 Coplen, T. B. (1988). Normalization of oxygen and hydrogen isotope data. *Chemical Geology: Isotope
269 Geoscience Section*, 72(4):293–297.
- 270 Craig, H. (1961). Isotopic variations in meteoric waters. *Science*, 133(3465):1702–1703.
- 271 Dansgaard, W. (1964). Stable isotopes in precipitation. *Tellus*, 16(4):436–468.
- 272 De Graaf, S., Vonhof, H. B., Weissbach, T., Wassenburg, J. A., Levy, E. J., Kluge, T., and Haug, G. H. (2020).
273 A comparison of isotope ratio mass spectrometry and cavity ring-down spectroscopy techniques for
274 isotope analysis of fluid inclusion water. *Rapid Communications in Mass Spectrometry*, 34(16):e8837.
- 275 Evans, M. N., Tolwinski-Ward, S. E., Thompson, D. M., and Anchukaitis, K. J. (2013). Applications of proxy
276 system modeling in high resolution paleoclimatology. *Quaternary Science Reviews*, 76:16–28.

- 277 Fan, Y., Shi, X., Duan, Q., and Yu, L. (2022). Towards reliable uncertainty quantification for hydrologic
278 predictions, Part I: Development of a particle copula Metropolis Hastings method. *Journal of Hydrology*,
279 612:128163.
- 280 Ferijal, T., Batelaan, O., and Shanafield, M. (2021). Spatial and temporal variation in rainy season droughts
281 in the Indonesian Maritime Continent. *Journal of Hydrology*, 603:126999.
- 282 Funk, C., Peterson, P., Landsfeld, M., Pedreros, D., Verdin, J., Shukla, S., Husak, G., Rowland, J., Harrison, L.,
283 Hoell, A., et al. (2015). The climate hazards infrared precipitation with stations—a new environmental
284 record for monitoring extremes. *Scientific data*, 2(1):1–21.
- 285 Gao, C. and Li, G. (2023). Asymmetric effect of enso on the maritime continent precipitation in decaying
286 summers. *Climate Dynamics*, 61:2839–2852.
- 287 Godfrey, J. S. (1996). The effect of the Indonesian throughflow on ocean circulation and heat exchange with
288 the atmosphere: A review. *Journal of Geophysical Research: Oceans*, 101(C5):12217–12237.
- 289 Hastings, W. K. (1970). Monte Carlo sampling methods using Markov chains and their applications.
290 *Biometrika*, 57(1):97–109.
- 291 He, S., Goodkin, N. F., Jackisch, D., Ong, M. R., and Samanta, D. (2018a). Continuous real-time analysis of
292 the isotopic composition of precipitation during tropical rain events: Insights into tropical convection.
293 *Hydrological Processes*, 32(11):1531–1545.
- 294 He, S., Goodkin, N. F., Kurita, N., Wang, X., and Rubin, C. M. (2018b). Stable isotopes of precipitation during
295 tropical Sumatra Squalls in Singapore. *Journal of Geophysical Research: Atmospheres*, 123(7):3812–3829.
- 296 He, S., Jackisch, D., Samanta, D., Yi, P. K. Y., Liu, G., Wang, X., and Goodkin, N. F. (2021). Understanding
297 tropical convection through triple oxygen isotopes of precipitation from the maritime continent. *Journal*
298 *of Geophysical Research: Atmospheres*, 126(4):e2020JD033418.
- 299 Herho, S. H. S. (2022). A Univariate Extreme Value Analysis and Change Point Detection of Monthly Dis-
300 charge in Kali Kupang, Central Java, Indonesia. *JOIV: International Journal on Informatics Visualization*,
301 6(4):862–868.
- 302 Hornberger, G. M. (1995). New manuscript guidelines for the reporting of stable hydrogen, carbon, and
303 oxygen isotope ratio data. *Water Resources Research*, 31(12):2895–2895.
- 304 Hu, C., Lian, T., Cheung, H.-N., Qiao, S., Li, Z., Deng, K., Yang, S., and Chen, D. (2020). Mixed diversity
305 of shifting IOD and El Niño dominates the location of Maritime Continent autumn drought. *National*
306 *Science Review*, 7(7):1150–1153.
- 307 Hudson, J. and Maloney, E. (2023). The Role of Surface Fluxes in MJO Propagation through the Maritime
308 Continent. *Journal of Climate*, 36(6):1633–1652.
- 309 Hutchings, J. A. and Konecky, B. L. (2023). Optimization of a Picarro L2140-i cavity ring-down spectrometer
310 for routine measurement of triple oxygen isotope ratios in meteoric waters. *Atmospheric Measurement*
311 *Techniques*, 16(6):1663–1682.
- 312 Jackisch, D., Yeo, B. X., Switzer, A. D., He, S., Cantarero, D. L. M., Siringan, F. P., and Goodkin, N. F. (2022).
313 Precipitation stable isotopic signatures of tropical cyclones in Metropolitan Manila, Philippines, show
314 significant negative isotopic excursions. *Natural Hazards and Earth System Sciences*, 22(1):213–226.
- 315 Jones, G. L. and Qin, Q. (2022). Markov chain Monte Carlo in practice. *Annual Review of Statistics and Its*
316 *Application*, 9:557–578.
- 317 Kang, X., Niu, Y., Yu, H., Gou, P., Hou, Q., Lu, X., and Wu, Y. (2022). Effect of rainfall-runoff process on
318 sources and transformations of nitrate using a combined approach of dual isotopes, hydrochemical and
319 Bayesian model in the Dagang River basin. *Science of the Total Environment*, 837:155674.
- 320 Karras, C., Karras, A., Avlonitis, M., and Sioutas, S. (2022). An overview of mcmc methods: From theory
321 to applications. In *IFIP International Conference on Artificial Intelligence Applications and Innovations*,
322 pages 319–332. Springer.
- 323 Klauenberg, K., Wübbeler, G., Mickan, B., Harris, P., and Elster, C. (2015). A tutorial on Bayesian normal
324 linear regression. *Metrologia*, 52(6):878.

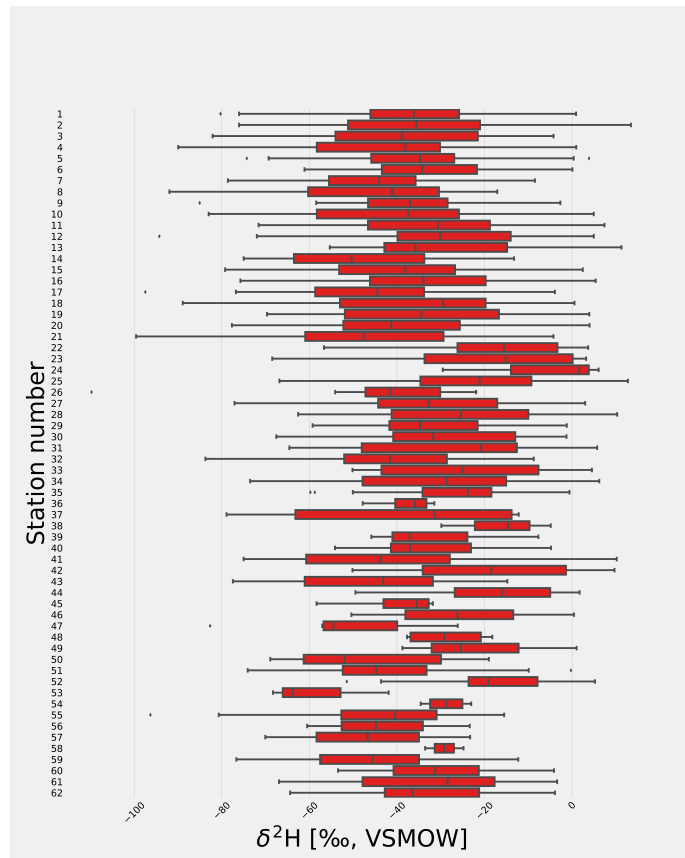
- 325 Kurita, N., Ichiyanagi, K., Matsumoto, J., Yamanaka, M. D., and Ohata, T. (2009). The relationship between
326 the isotopic content of precipitation and the precipitation amount in tropical regions. *Journal of Geo-*
327 *chemical Exploration*, 102(3):113–122.
- 328 Li, M., Gordon, A. L., Gruenburg, L. K., Wei, J., and Yang, S. (2020). Interannual to decadal response
329 of the Indonesian throughflow vertical profile to Indo-Pacific forcing. *Geophysical Research Letters*,
330 47(11):e2020GL087679.
- 331 Liu, J. Y., Zhang, F. P., Feng, Q., Wei, Y. F., Huang, L. H., Li, Z. X., Nie, S., and Li, L. (2019). Stable isotopes
332 characteristics of precipitation over Shaanxi-Gansu-Ningxia and its water vapor sources. *The Journal of*
333 *Applied Ecology*, 30(7):2191–2200.
- 334 Lu, J., Li, T., and Shen, X. (2023). Precipitation diurnal cycle over the maritime continent modulated by
335 ENSO. *Climate Dynamics*, 61:2547–2564.
- 336 Maithani, S. and Pradhan, M. (2020). Cavity ring-down spectroscopy and its applications to environmental,
337 chemical and biomedical systems. *Journal of Chemical Sciences*, 132:1–19.
- 338 Makarim, S., Sprintall, J., Liu, Z., Yu, W., Santoso, A., Yan, X.-H., and Susanto, R. D. (2019). Previously uniden-
339 tified Indonesian Throughflow pathways and freshening in the Indian Ocean during recent decades. *Sci-*
340 *entific Reports*, 9(1):7364.
- 341 Malik, F., Butt, S., and Mujahid, N. (2022). Variation in isotopic composition of precipitation with identifica-
342 tion of vapor source using deuterium excess as tool. *Journal of Radioanalytical and Nuclear Chemistry*,
343 pages 1–8.
- 344 Mao, H., Wang, C., Qu, S., Liao, F., Wang, G., and Shi, Z. (2023). Source and evolution of sulfate in the multi-
345 layer groundwater system in an abandoned mine—Insight from stable isotopes and Bayesian isotope
346 mixing model. *Science of the Total Environment*, 859:160368.
- 347 Mäs, S., Henzen, D., Bernard, L., Müller, M., Jirka, S., and Senner, I. (2018). Generic schema descriptions
348 for comma-separated values files of environmental data. In *The 21th AGILE International Conference on*
349 *Geographic Information Science*.
- 350 McKinney, W. et al. (2011). pandas: a foundational Python library for data analysis and statistics. *Python*
351 *for high performance and scientific computing*, 14(9):1–9.
- 352 Merlivat, L. and Jouzel, J. (1979). Global climatic interpretation of the deuterium-oxygen 18 relationship for
353 precipitation. *Journal of Geophysical Research: Oceans*, 84(C8):5029–5033.
- 354 Metropolis, N., Rosenbluth, A. W., Rosenbluth, M. N., Teller, A. H., and Teller, E. (1953). Equation of state
355 calculations by fast computing machines. *The Journal of Chemical Physics*, 21(6):1087–1092.
- 356 Munksgaard, N. C., Kurita, N., Sánchez-Murillo, R., Ahmed, N., Araguas, L., Balachew, D. L., Bird, M. I.,
357 Chakraborty, S., Chinh, N. K., Cobb, K. M., et al. (2019). Data descriptor: Daily observations of stable
358 isotope ratios of rainfall in the tropics. *Scientific Reports*, 9(1):14419.
- 359 Nagai, T., Hibiya, T., and Syamsudin, F. (2021). Direct estimates of turbulent mixing in the Indonesian
360 archipelago and its role in the transformation of the Indonesian throughflow waters. *Geophysical Re-*
361 *search Letters*, 48(6):e2020GL091731.
- 362 Nan, Y., He, Z., Tian, F., Wei, Z., and Tian, L. (2021). Can we use precipitation isotope outputs of isotopic
363 general circulation models to improve hydrological modeling in large mountainous catchments on the
364 Tibetan Plateau? *Hydrology and Earth System Sciences*, 25(12):6151–6172.
- 365 Peatman, S. C., Schwendike, J., Birch, C. E., Marsham, J. H., Matthews, A. J., and Yang, G.-Y. (2021). A local-
366 to-large scale view of Maritime Continent rainfall: Control by ENSO, MJO, and equatorial waves. *Journal*
367 *of Climate*, 34(22):8933–8953.
- 368 Peng, P., Zhang, X. J., and Chen, J. (2020). Bias correcting isotope-equipped GCMs outputs to build precip-
369 itation oxygen isoscape for eastern China. *Journal of Hydrology*, 589:125153.
- 370 Perkel, J. (2016). Democratic databases: science on GitHub. *Nature*, 538(7623):127–128.
- 371 Pfahl, S. and Sodemann, H. (2014). What controls deuterium excess in global precipitation? *Climate of the*
372 *Past*, 10(2):771–781.

- 373 Putman, A. L., Fiorella, R. P., Bowen, G. J., and Cai, Z. (2019). A global perspective on local meteoric wa-
 374 ter lines: Meta-analytic insight into fundamental controls and practical constraints. *Water Resources*
 375 *Research*, 55(8):6896–6910.
- 376 Routson, C. C., McKay, N. P., Kaufman, D. S., Erb, M. P., Goosse, H., Shuman, B. N., Rodysill, J. R., and Ault,
 377 T. (2019). Mid-latitude net precipitation decreased with Arctic warming during the Holocene. *Nature*,
 378 568(7750):83–87.
- 379 Rozanski, K., Araguás-Araguás, L., and Gonfiantini, R. (1993). Isotopic patterns in modern global precipita-
 380 tion. *Climate change in continental isotopic records*, 78:1–36.
- 381 Sagayama, H., Racine, N. M., Shriver, T. C., and Schoeller, D. A. (2021). Comparison of isotope ratio
 382 mass spectrometry and cavity ring-down spectroscopy procedures and precision of the doubly labeled
 383 water method in different physiological specimens. *Rapid Communications in Mass Spectrometry*,
 384 35(21):e9188.
- 385 Salvatier, J., Wiecki, T. V., and Fonnesbeck, C. (2016). Probabilistic programming in Python using PyMC3.
 386 *PeerJ Computer Science*, 2:e55.
- 387 Sánchez-Murillo, R., Durán-Quesada, A. M., Birkel, C., Esquivel-Hernández, G., and Boll, J. (2017). Trop-
 388 ical precipitation anomalies and d-excess evolution during El Niño 2014-16. *Hydrological Processes*,
 389 31(4):956–967.
- 390 Santoso, A., England, M. H., Kajtar, J. B., and Cai, W. (2022). Indonesian Throughflow Variability and Linkage
 391 to ENSO and IOD in an Ensemble of CMIP5 Models. *Journal of Climate*, 35(10):3161–3178.
- 392 Shao, L., Tian, L., Cai, Z., Wang, C., and Li, Y. (2021). Large-scale atmospheric circulation influences the ice
 393 core d-excess record from the central Tibetan Plateau. *Climate Dynamics*, 57(7-8):1805–1816.
- 394 Sharma, S. and Mujumdar, P. P. (2022). Modeling concurrent hydroclimatic extremes with parametric mul-
 395 tivariate extreme value models. *Water Resources Research*, 58(2):e2021WR031519.
- 396 South, L. F., Riabiz, M., Teymur, O., and Oates, C. J. (2022). Postprocessing of MCMC. *Annual Review of*
 397 *Statistics and Its Application*, 9:529–555.
- 398 Supari, Tangang, F., Salimun, E., Aldrian, E., Sopaheluwakan, A., and Juneng, L. (2018). ENSO modulation
 399 of seasonal rainfall and extremes in Indonesia. *Climate Dynamics*, 51:2559–2580.
- 400 Suwarman, R., Ichiyanagi, K., Tanoue, M., Yoshimura, K., Mori, S., Yamanaka, M. D., Kurita, N., and Syam-
 401 sudin, F. (2013). The variability of stable isotopes and water origin of precipitation over the Maritime
 402 Continent. *SOLA*, 9:74–78.
- 403 Suwarman, R., Ichiyanagi, K., Tanoue, M., Yoshimura, K., Mori, S., Yamanaka, M. D., Syamsudin, F., and Bel-
 404 gaman, H. A. (2017). El niño southern oscillation signature in atmospheric water isotopes over maritime
 405 continent during wet season. *Journal of the Meteorological Society of Japan. Ser. II*, 95(1):49–66.
- 406 Taylor, D. (2015). Work the shell: analyzing comma-separated values (csv) files. *Linux Journal*, 2015(260):3.
- 407 Torres-Martínez, J. A., Mora, A., Knappett, P. S. K., Ornelas-Soto, N., and Mahlknecht, J. (2020). Tracking
 408 nitrate and sulfate sources in groundwater of an urbanized valley using a multi-tracer approach combined
 409 with a bayesian isotope mixing model. *Water Research*, 182:115962.
- 410 Tritschler, F., Binder, M., Händel, F., Burghardt, D., Dietrich, P., and Liedl, R. (2020). Collected Rain Water
 411 as Cost-Efficient Source for Aquifer Tracer Testing. *Groundwater*, 58(1):125–131.
- 412 Uieda, L., Tian, D., Leong, W. J., Schlitzer, W., Grund, M., Jones, M., Fröhlich, Y., Toney, L., Yao, J., Magen,
 413 Y., Tong, J.-H., Materna, K., Belem, A., Newton, T., Anant, A., Ziebarth, M., Quinn, J., and Wessel, P.
 414 (2023). PyGMT: A Python interface for the Generic Mapping Tools. Software available from <https://doi.org/10.5281/zenodo.7772533>.
 415
- 416 Valdivielso, S., Vázquez-Suñé, E., and Custodio, E. (2020). Origin and variability of oxygen and hydrogen
 417 isotopic composition of precipitation in the Central Andes: A review. *Journal of Hydrology*, 587:124899.
- 418 Van Der Walt, S., Colbert, S. C., and Varoquaux, G. (2011). The NumPy array: a structure for efficient nu-
 419 merical computation. *Computing in science & engineering*, 13(2):22–30.
- 420 Vinnarasí, R. and Dhanya, C. T. (2022). Time-varying Intensity-Duration-Frequency relationship through
 421 climate-informed covariates. *Journal of Hydrology*, 604:127178.

- 422 Wei, Y., Pu, Z., and Zhang, C. (2020). Diurnal cycle of precipitation over the Maritime Continent under mod-
423 ulation of MJO: Perspectives from cloud-permitting scale simulations. *Journal of Geophysical Research:*
424 *Atmospheres*, 125(13):e2020JD032529.
- 425 Wessel, P., Luis, J. F., Uieda, L., Scharroo, R., Wobbe, F., Smith, W. H. F., and Tian, D. (2019). The Generic
426 Mapping Tools Version 6. *Geochemistry, Geophysics, Geosystems*, 20(11):5556–5564.
- 427 West, M. (1984). Outlier models and prior distributions in Bayesian linear regression. *Journal of the Royal*
428 *Statistical Society Series B: Statistical Methodology*, 46(3):431–439.
- 429 Xia, C., Liu, G., Chen, K., Hu, Y., Zhou, J., Liu, Y., and Mei, J. (2020). Stable isotope characteristics for
430 precipitation events and their responses to moisture and environmental changes during the summer
431 monsoon period in southwestern china. *Polish Journal of Environmental Studies*, 29(3).
- 432 Xia, C., Liu, G., Mei, J., Meng, Y., Liu, W., and Hu, Y. (2019a). Characteristics of hydrogen and oxygen stable
433 isotopes in precipitation and the environmental controls in tropical monsoon climatic zone. *International*
434 *Journal of Hydrogen Energy*, 44(11):5417–5427.
- 435 Xia, C. C., Chen, K., Zhou, J., Mei, J., Liu, Y. P., and Liu, G. D. (2019b). Comparison of precipitation stable
436 isotopes during wet and dry seasons in a subtropical monsoon climate region of China. *Applied Ecology*
437 *& Environmental Research*, 17(5).
- 438 Xiao, H.-M., Lo, M.-H., and Yu, J.-Y. (2022). The increased frequency of combined El Niño and positive IOD
439 events since 1965s and its impacts on maritime continent hydroclimates. *Scientific Reports*, 12(1):7532.
- 440 Xu, H., Song, S., Guo, T., and Wang, H. (2022). Two-stage hybrid model for hydrological series prediction
441 based on a new method of partitioning datasets. *Journal of Hydrology*, 612:128122.
- 442 Xue, P., Malanotte-Rizzoli, P., Wei, J., and Eltahir, E. A. B. (2020). Coupled ocean-atmosphere modeling over
443 the Maritime Continent: A review. *Journal of Geophysical Research: Oceans*, 125(6):e2019JC014978.
- 444 Yamanaka, M. D. (2016). Physical climatology of Indonesian maritime continent: An outline to comprehend
445 observational studies. *Atmospheric Research*, 178:231–259.
- 446 Yang, S., Zhang, T., Li, Z., and Dong, S. (2019). Climate variability over the maritime continent and its role
447 in global climate variation: A review. *Journal of Meteorological Research*, 33(6):993–1015.
- 448 Yoshikawa, K., Úbeda, J., Masías, P., Pari, W., Apaza, F., Vasquez, P., Ccallata, B., Concha, R., Luna, G., Ipar-
449 raguirre, J., et al. (2020). Current thermal state of permafrost in the southern Peruvian Andes and poten-
450 tial impact from El Niño–Southern Oscillation (ENSO). *Permafrost and Periglacial Processes*, 31(4):598–
451 609.
- 452 Zaryab, A., Nassery, H. R., Knoeller, K., Alijani, F., and Minet, E. (2022). Determining nitrate pollution sources
453 in the Kabul Plain aquifer (Afghanistan) using stable isotopes and Bayesian stable isotope mixing model.
454 *Science of the Total Environment*, 823:153749.
- 455 Zhang, J. and Xu, Z. (2023). Vacuum extraction of high-salinity water for the determination of oxygen and hy-
456 drogen isotopic compositions using cavity ring-down spectroscopy. *Microchemical Journal*, 190:108678.
- 457 Zhang, Q., Wang, H., and Lu, C. (2020). Tracing sulfate origin and transformation in an area with multiple
458 sources of pollution in northern China by using environmental isotopes and Bayesian isotope mixing
459 model. *Environmental Pollution*, 265:115105.
- 460 Zhu, J., Guan, Z., and Wang, X. (2022). Variations of Summertime SSTA Independent of ENSO in the Mar-
461 itime Continent and Their Possible Impacts on Rainfall in the Asian–Australian Monsoon Region. *Journal*
462 *of Climate*, 35(24):7949–7964.
- 463 Zolghadr-Asli, B., Bozorg-Haddad, O., Enayati, M., and Loáiciga, H. A. (2022). Sensitivity of non-conditional
464 climatic variables to climate-change deep uncertainty using Markov Chain Monte Carlo simulation. *Sci-*
465 *entific Reports*, 12(1):1813.

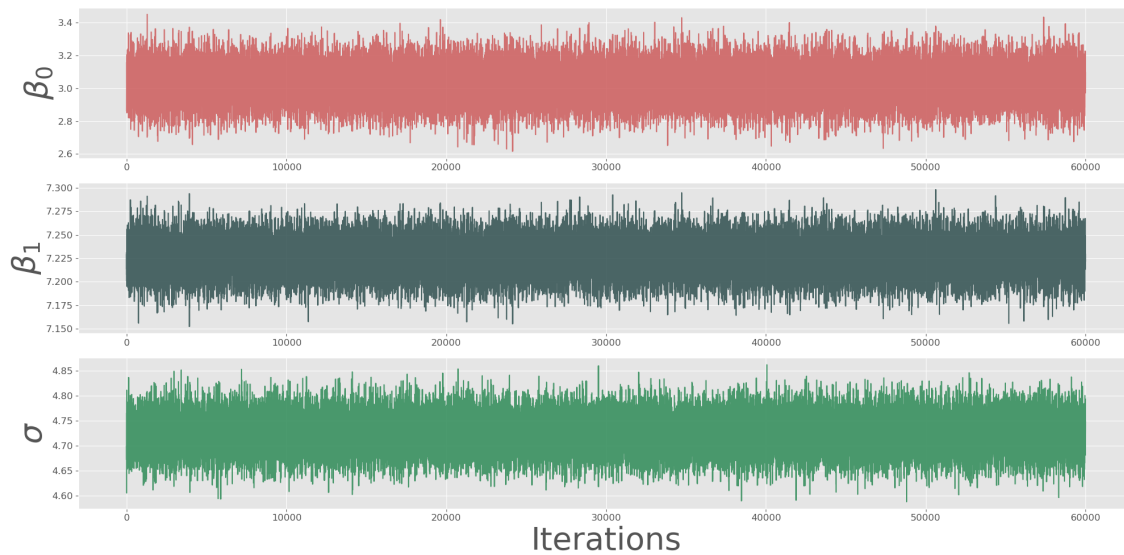


(a)

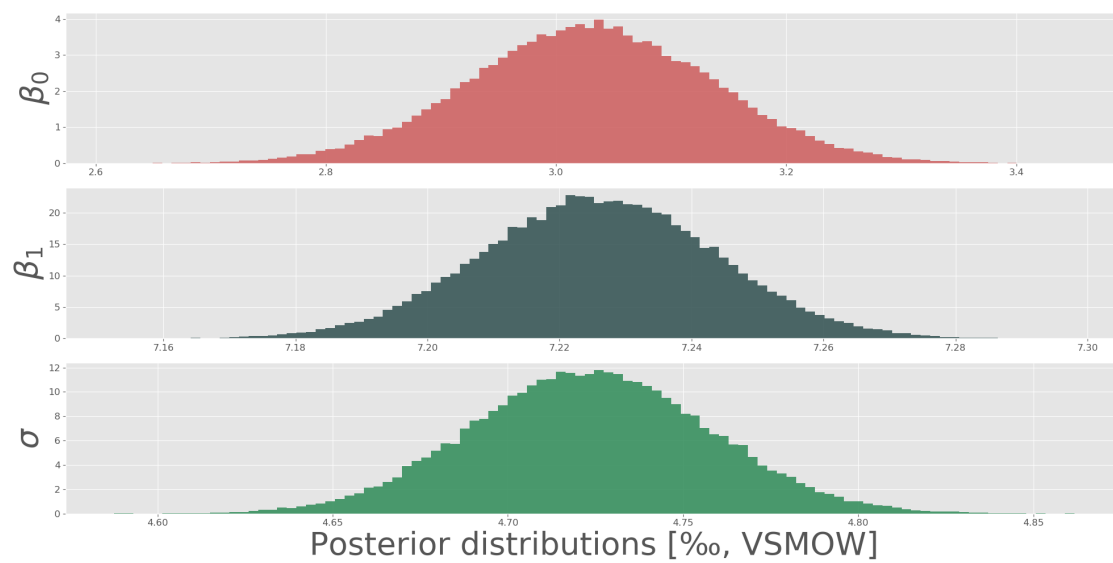


(b)

Figure 3: Box plots of the monthly (a) $\delta^{18}\text{O}$ and (b) $\delta^2\text{H}$ recorded by the 62 stations between September 2010 and September 2017.



(a)



(b)

Figure 4: (a) BLR posterior parameter trace plots for the intercept (upper panel), slope (middle panel), and standard deviation (lower panel). (b) Posterior distribution of the three linear regression parameters: intercept (upper panel), slope (middle panel), and standard deviation (lower panel).

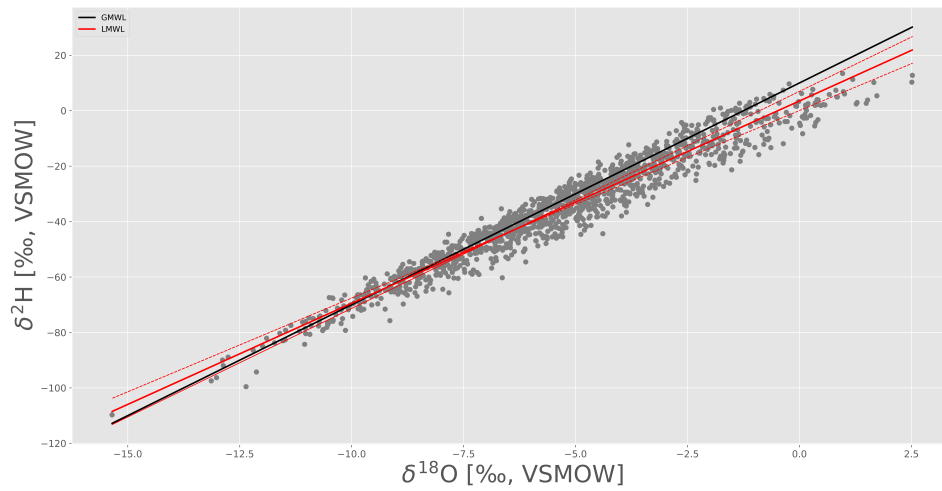


Figure 5: The GMWL (solid black line) compared to the LMWL (the posterior mean shown by a solid red line, area between the dashed red lines shows 95% credible interval obtained from the highest posterior density interval (HPDI)) of all stations over the IMC. Grey dots indicate individual data points.